Temporal evolution and electric potential structure of the auroral acceleration region from multispacecraft measurements

Article

Published Version

Temporal evolution and electric potential structure of the auroral acceleration region from multispacecraft measurements

C. Forsyth,[1] A. N. Fazakerley,[1] A. P. Walsh,[1] C. E. J. Watt,[2] K. J. Garza,[1] C. J. Owen,[1] D. Constantinescu,[3] I. Dandouras,[4] K.-H. Fornaçon,[3] E. Lucek,[5] G. T. Marklund,[6] S. S. Sadeghi,[6] Y. Khotyaintsev,[7] A. Masson,[8] and N. Doss[1]

Received 24 February 2012; revised 11 October 2012; accepted 12 October 2012; published 6 December 2012.

[1] Bright aurorae can be excited by the acceleration of electrons into the atmosphere in violation of ideal magnetohydrodynamics. Modeling studies predict that the accelerating electric potential consists of electric double layers at the boundaries of an acceleration region but observations suggest that particle acceleration occurs throughout this region. Using multispacecraft observations from Cluster, we have examined two upward current regions on 14 December 2009. Our observations show that the potential difference below C4 and C3 changed by up to 1.7 kV between their respective crossings, which were separated by 150 s. The field-aligned current density observed by C3 was also larger than that observed by C4. The potential drop above C3 and C4 was approximately the same in both crossings. Using a novel technique of quantitively comparing the electron spectra measured by Cluster 1 and 3, which were separated in altitude, we determine when these spacecraft made effectively magnetically conjugate observations, and we use these conjugate observations to determine the instantaneous distribution of the potential drop in the AAR. Our observations show that an average of 15% of the potential drop in the AAR was located between C1 at 6235 km and C3 at 4685 km altitude, with a maximum potential drop between the spacecraft of 500 V, and that the majority of the potential drop was below C3. Assuming a spatial invariance along the length of the upward current region, we discuss these observations in terms of temporal changes and the vertical structure of the electrostatic potential drop and in the context of existing models and previous single- and multispacecraft observations.

Citation: Forsyth, C., et al. (2012), Temporal evolution and electric potential structure of the auroral acceleration region from multispacecraft measurements, *J. Geophys. Res.*, *117*, A12203, doi:10.1029/2012JA017655.

1. Introduction

[2] Aurorae can be caused by the collisional excitation of ionospheric particles by charged particles, predominantly electrons, accelerated or scattered out of the magnetosphere. The majority of magnetospheric electrons are trapped in the magnetosphere through the conservation of the first adiabatic invariant in the geometry of Earth's magnetic field (magnetic mirroring). These electrons can only escape into the atmosphere when their equatorial pitch angle approaches 0° or 180° such that they are inside the loss cone. Electrons that are pitch angle scattered by electromagnetic chorus waves cause dim, diffuse aurorae [*Thorne et al.*, 2010]. Electrons accelerated along the magnetic field to keV energies by magnetic field-aligned electric fields, either from quasi-static potential drops [*McIlwain*, 1960; *Carlqvist and Boström*, 1970; *Frank and Ackerson*, 1971; *Mozer et al.*, 1977, 1980; *Lyons et al.*, 1979; *Reiff et al.*, 1988; *Mozer and Kletzing*, 1998] or from low-frequency Alfvén waves with short perpendicular scales [*Hasegawa*, 1976; *Goertz and Boswell*, 1979; *Lysak and Carlson*, 1981; *Lysak and Dum*, 1983; *Wygant et al.*, 2000; *Keiling et al.*, 2002; *Watt et al.*, 2005; *Chaston et al.*, 2007] produce bright aurora. Acceleration through quasi-static potential drops takes place at altitudes in the range 1,400–14,000 km [*Reiff et al.*, 1988; *Lindqvist and Marklund*, 1990; *Lu et al.*, 1992] in a region called the auroral acceleration region (AAR).

[1]Mullard Space Science Laboratory, University College London, Dorking, UK.
[2]Department of Physics, University of Alberta, Edmonton, Alberta, Canada.
[3]Institut fur Geophysik und Meteorologie, Technische Universität Braunschweig, Braunschweig, Germany.
[4]Institut de Recherche en Astrophysique et Planétologie, CNRS, University of Toulouse, Toulouse, France.
[5]Blackett Laboratory, Imperial College London, London, UK.
[6]School of Electrical Engineering, Royal Institute of Technology, Stockholm, Sweden.
[7]Swedish Institute of Space Physics, Uppsala, Sweden.
[8]Science Operations Department, European Space Agency/European Space Research and Technology Centre, Noordwijk, Netherlands.

Corresponding author: C. Forsyth, Mullard Space Science Laboratory, University College London, Holmbury St. Mary, Dorking RH5 6NT, UK. (cfo@mssl.ucl.ac.uk)

0148-0227/12/2012JA017655

[3] Mono-energetic electron distributions seen in regions of upward field-aligned current have been associated with quasi-static potential drops forming U or S shaped structures [*Mozer et al.*, 1980; *Lindqvist and Marklund*, 1990; *Marklund et al.*, 2011a, 2011b; *Sadeghi et al.*, 2011] in the AAR. Vlasov models of this region [*Ergun et al.*, 2000] suggest that this potential is concentrated in two strong electric double layers [*Block*, 1972] at the upper and lower boundaries of the acceleration region. A statistical study has shown that double layers at the bottom of the AAR can contain 10%–50% of the total potential drop [*Ergun et al.*, 2002]. Double layers within the AAR were not present in the models but have been observed by spacecraft [*Ergun et al.*, 2004]. Furthermore, it has been suggested that the fine structure of auroral kilometric radiation (AKR) is related to moving electrostatic shocks or oblique double layers inside the AAR [*Pottelette et al.*, 2003]. However, the Vlasov simulations of *Ergun et al.* [2000] also showed that a small proportion of the potential was distributed throughout the AAR. These studies suggest that particle acceleration occurs both in distinct steps and gradually throughout the region.

[4] Dedicated single spacecraft missions, such as Viking, Freja, FAST and Polar, have offered insights into the localised physical processes within the AAR. However, for practical reasons, single spacecraft data are of limited use in determining the temporal evolution and spatial structure of the AAR. *Mozer and Hull* [2001] showed that, statistically, the fraction of the electric potential drop along the magnetic field below a given location tends to decrease with altitude. Similarly, *Olsson and Janhunen* [2003] showed that the absolute value of the potential drop below a spacecraft's height decreased with altitude and, along with *Hull et al.* [2003], showed that the magnetic field-aligned electric field (potential gradient) tended to be larger at lower altitudes.

[5] Previous multispacecraft or multimission studies of the AAR have used spacecraft separated by large distances (>10,000 km), typically with only one spacecraft in the AAR. These studies have shown that particles are accelerated by quasi-static electric fields [*Reiff et al.*, 1988] and that the altitude at which ions are accelerated is around 1700 km for large potential drops, but increases to 2000–2500 km for small potential drops [*Reiff et al.*, 1993]. Combining FAST and Polar data in a small number of case studies, *Janhunen et al.* [2001] showed that low-potential-drop inverted-V signatures at FAST (1900–4100 km altitude) tended to be associated with a Maxwellian electron source population at Polar (20,000–37,000 km) and that broadband electrostatic wave activity was well correlated with the acceleration of cold electrons when the source distribution was non-Maxwellian.

[6] Recent observations by Cluster have, for the first time, provided observations within the AAR at heights separated by less than a few thousand kilometers. *Marklund et al.* [2011a] and *Sadeghi et al.* [2011] have examined AAR crossings on the dayside and nightside respectively during which two or three of the Cluster spacecraft passed through the quasi-static AAR within a few minutes of each other and at slightly different heights. By assuming that each individual AAR was temporally invariant during these events, based on the same total potential drop being observed, these studies showed that the potential drop between the two spacecraft in the AAR had values between 0.6 and 4 kV. The potential structure in the dayside AAR studied by *Marklund et al.* [2011a] appeared to be invariant on a timescale of at least 5 min whereas the potential structures in the nightside upward current AARs examined by *Sadeghi et al.* [2011] showed variations on a timescale of 40–100 s.

[7] In this study, we present the first observations from a period when three of the Cluster spacecraft passed through an AAR with one pair of the spacecraft separated along their orbit and another pair of spacecraft coming into magnetic conjugacy during the AAR crossing. The multispacecraft data enable us to simultaneously make observations of the plasma populations at two different heights within the AAR separated by ~1,500 km and to determine the temporal variation of the AAR. We compare the particle populations at two altitudes to identify those periods in which the spacecraft were magnetically conjugate. We use these data to examine the acceleration of the particle population and to determine the potential and the average electric field between the spacecraft, as well as above the spacecraft pair. We also compare the field-aligned current densities and potential drops above and below the spacecraft to determine the temporal variability of the AAR. These results are presented in the context of recent multispacecraft studies and previous single-spacecraft statistical studies.

2. Instrumentation and Spacecraft Locations

[8] The Cluster mission consists of four identically instrumented spacecraft launched into closely separated, highly elliptical polar orbits of the Earth. In-flight manoeuvres optimize the spacecraft formation for making 3-D measurements of the local plasma environment in specific regions. In 2008, the spacecraft were manoeuvred to allow short intervals of magnetic conjugacy between Cluster 1 (C1) and Cluster 3 (C3) or Cluster (C4) during crossings of the predicted auroral oval. In practice, only a fraction of these conjugate intervals coincided with passages through an active AAR. Here we present an event in which the spacecraft were very close to conjugacy as they crossed the AAR.

[9] Figure 1a shows the position of the spacecraft in GSM (Geocentric Solar Magnetospheric) coordinates at 10:46 UT on 14 December 2009 during the event that we present here. The spacecraft were moving predominantly westward. A magnetic field model [*Tsyganenko and Stern*, 1996] shows that C1 and C3 were close to magnetic conjugacy during the event (Figure 1a, dotted line). Figure 1b shows the spacecraft foot points between 10:40 and 10:50 UT in MLAT/MLT coordinates. The magnetic foot points of C1, C3 and C4 were at approximately 70° invariant latitude throughout while C2 was further poleward. Figure 1c shows the separation of C1 and C3 perpendicular to the model magnetic field and that their closest separation across the model field was ~100 km at 10:45:57 UT (Figure 1c). Between 10:44 and 10:47 UT, C1 and C3 were separated along the model magnetic field by between 1850 and 1475 km (C1 at higher altitude). C4 was on the same orbit as C3, but leading C3 by 192 s. C2 was at a higher magnetic latitude and data from this spacecraft show it was inside the polar cap throughout the interval of interest. The spacecraft crossing of the AAR occurred at around 1 MLT and nearly 2 hours after a substorm onset, identified from auroral electrojet activity indices (not shown), when the AE index was <70 nT and the AL index was >−20 nT.

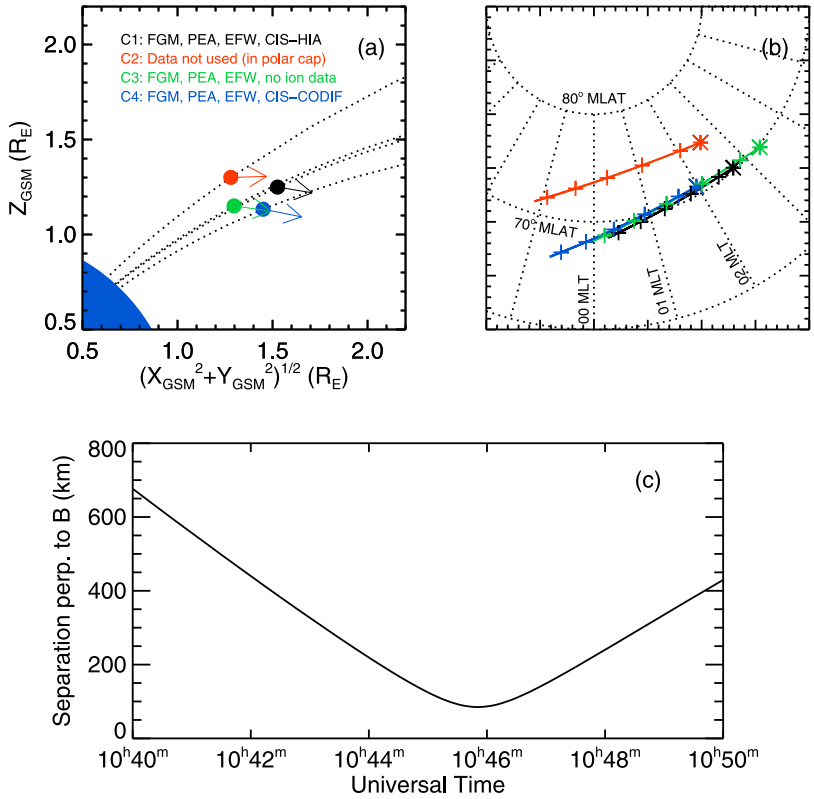

Figure 1. (a) Locations of the Cluster spacecraft in GSM coordinates (C1, black; C2, red; C3, green; C4, blue) at 10:46 UT. The dotted lines show the model magnetic field lines. The arrows indicate the directions of travel of the spacecraft. (b) The foot points of the spacecraft in MLT and invariant latitude (MLAT) coordinates between 10:40 and 10:50 UT. The asterisks indicate the start positions of the spacecraft, and the crosses indicate their position every 2 minutes. The spacecraft were moving tailward and westward, covering approximately 4 hours of magnetic local time between 10:40 and 10:50 UT. (c) The separation of C1 and C3 perpendicular to the model magnetic field direction. C1 and C3 were closest to a model conjugacy at 10:45:57 UT.

[10] In this study we use data from the Cluster Ion Spectrometer (CIS) [*Rème et al.*, 2001], Fluxgate Magnetometer (FGM) [*Balogh et al.*, 2001], Electric Field and Wave instrument (EFW) [*Gustafsson et al.*, 2001] and Plasma Electron And Current Experiment (PEACE) [*Johnstone et al.*, 1997] on Cluster. CIS data were not available from C3. CIS ion data were available only from the Hot Ion Analyzer (HIA) on C1 or the Composition Distribution Function sensor (CODIF) on C4; thus we cannot compare either conjugate ion measurements or ion measurements at the same altitude. We can, however, compare the electric potential change below the spacecraft inferred from the ion and electric field measurements and use the available ion measurements to show the acceleration of ionospheric particles into the magnetosphere. The two PEACE sensors (HEEA and LEEA, with fields-of-view separated by 180° in the spacecraft spin plane) had fully overlapping energy ranges during this interval and, as such, we were able to determine the 2-D pitch angle distribution of the electrons every half-spin (2 s). Electron moments were calculated from the PEACE 3DX data using the latest available ground calibrations [*Fazakerley et al.*, 2010]. The spacecraft were operating in a "burst" telemetry mode so these 3-D electron distributions were available at 4 s cadence. The EFW instrument measures the electric field in the spacecraft spin plane using spherical sensors deployed orthogonally on 44 m long wire booms in the spin plane of the spacecraft. The two pairs of opposing sensors, separated by 88 m tip-tip, provide two orthogonal components of the electric field. The failure of one of the sensors on C2 and C3 prior to the time of our event results in somewhat reduced data quality. The failure of two of the sensors on C1 prior to our event means that only one component of E in the spin plane is measured, and that the 2-D electric field can be measured only at spin resolution [*Khotyaintsev et al.*, 2010].

3. Observations of the Auroral Acceleration Region

[11] An overview of the AAR crossing by C1, C3 and C4 is presented in Figure 2. Data from the PEACE and CIS instruments on Cluster are plotted against the magnetic local time (MLT) of the spacecraft foot points, calculated from the *Tsyganenko and Stern* [1996] field model, which is approximately equivalent to the IGRF model at the altitude of the observations. Figure 2a shows the times at which the spacecraft passed over each MLT (note C1 crosses over C3). Figures 2b–2f show the phase space density of the upward

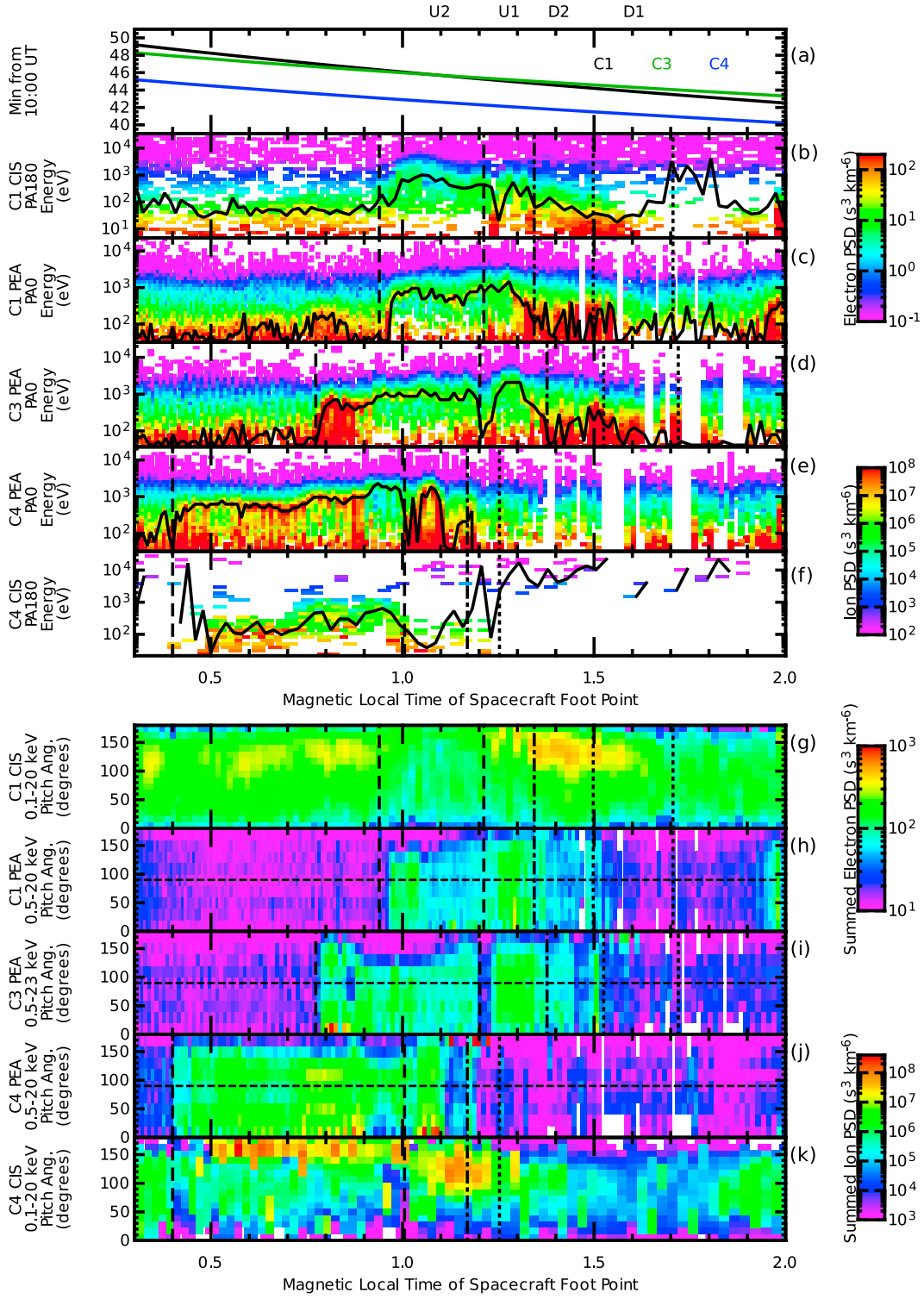

Figure 2. Data from C1, C3 and C4 as they passed through the AAR, plotted against MLT. (a) The times at which the spacecraft foot point was at each MLT. (b–f) Spectrograms of the phase space density of upgoing field-aligned ions from C1, down-going field-aligned electrons from C1, C3 and C4 and upgoing field-aligned ions from C4 respectively. (g–k) Spectrograms of the phase space density versus pitch angle of ions from C1, electrons from C1, C3 and C4, and H+ ions from C4. The black trace in Figures 2b and 2f shows the characteristic energy of the ions. The black traces in Figures 2c–2e show the energy of the peak of the phase space density of the electrons. The vertical lines delimit the upward (dashed) and downward (dotted) current systems identified from the field-aligned current densities (see Figure 3).

field-aligned ions detected by C1, the downward field-aligned electrons detected by C1, C3 and C4, and the upward field-aligned H+ ions detected by C4 respectively. Overlaid on the ion data is the ion characteristic energy in black (calculated as the total upgoing energy flux divided by the total upgoing number flux), which has previously been shown to be a good measure of the electric potential drop below the spacecraft [e.g. *Reiff et al.*, 1988; *McFadden et al.*, 1998, 1999]. Overlaid on the electron data is the energy of the peak of the phase space density distributions. Figures 2g–2k show the phase space density, summed over a range of energies and plotted against pitch angle and MLT, of the ions from C1, the electrons from C1, C3 and C4 and the H^+ ions from C4, respectively.

[12] The observations of the particles in the AAR are broadly consistent with previous in-situ measurements (for a review, see *Paschmann et al.* [2003]). C1, C3 and C4 all encountered an auroral acceleration region, indicated by the presence of energised ion and electron populations. The eastern side of the AAR (~1.3–1.7 MLT on C1 and C3 and ~1.1–1.35 on C4) was dominated by low energy electrons predominantly flowing away from the Earth (not shown) and low energy ion conics centred on pitch angles of 120°–130°, indicating a downward current region (delimited by vertical dotted lines in the figure). The western side of the AAR (~0.9–1.3 MLT on C1 and C3 and ~0.4–1.1 MLT on C4) contained downward-going electrons with a mono-energetic peaked distribution with peak energies of 300–2300 eV and field-aligned upward going ions with characteristic energies of up to 1 keV, indicating an upward current region (delimited by the dashed vertical lines in the figure). Ion composition data from C4 (not shown) shows that the presence of upgoing H^+, He^+ and O^+ ions in the upward current region, consistent with an ionospheric ion source.

[13] In the upward current region, data from the C3 and C4 PEACE instruments show two distinct electron structures; a relatively narrow (~0.1 MLT) structure to the east (1.2–1.3 MLT on C3 and 1–1.1 MLT on C4) and a wider (>0.3 MLT) structure to the west (0.9–1.2 MLT on C3 and 0.4–1 MLT on C4). These structures are separated by a dropout in the electron flux at 1.2 and 1 MLT on C3 and C4 respectively. The electron data from C1 indicate a single, continuous structure, although the ion data shows a flux dropout approximately co-located with the electron dropout on C3.

[14] Figure 3 shows the magnetic field data from C1, C3 and C4 as they passed over the auroral region. The top panels show the observed magnetic field in GSE coordinates. The middle panels show the residual magnetic field when the *Tsyganenko and Stern* [1996] magnetic field model is removed, plotted in two directions perpendicular to the model magnetic field direction (westward and northward). The bottom panels show the field-aligned current densities, which were calculated from the residual magnetic field data using a single spacecraft approximation of Ampére's law (black) [*Marchaudon et al.*, 2006] and from the electron moments (blue). The gradient of the component of the residual magnetic field perpendicular to the background field and the spacecraft velocity (in the $\mathbf{v}_{sc} \times \mathbf{b}$ direction) and the spacecraft velocity relative to the current system and perpendicular to the magnetic field (in the $\mathbf{b} \times \mathbf{v}_{sc} \times \mathbf{b}$ direction) give the field-aligned current density through Ampére's law, assuming that the current system is an infinite field-aligned current sheet. We do not use the curlometer technique [*Dunlop et al.*, 1988] because the Cluster tetrahedron was much larger than the current systems encountered and as such, the results of this technique would not be very precise [*Runov et al.*, 2005; *Forsyth et al.*, 2011]. The component of the field-aligned current calculated from the ion moments is not included as this was much smaller than from the electrons throughout the crossings.

[15] The field-aligned current densities determined from the FGM data showed similar features on the three spacecraft. From these data we identify 4 distinct current regions: two downward current regions (D1 and D2) and two upward current regions (U1 and U2). These are most clearly seen in the data from C3. Comparing the current densities, it appears that D1 was not observed by C4 (or was very weak), that D2 was bifurcated at C1 and U1 was bifurcated at C4 (indicated by the dot-dashed lines). The locations of these current systems matches the upward and downward current regions identified in the particle data and are delimited by the dashed (upward currents) and dotted (downward currents) vertical lines.

[16] Table 1 shows the maximum variance directions and ratio of the maximum and intermediate Eigenvalues determined using minimum variance analysis (MVA) [*Sonnerup and Cahill*, 1967; *Sonnerup and Scheible*, 1998] for each of the marked current sheets in Figure 3. Also shown are the angles between the maximum variance direction and the magnetic field direction, the perpendicular northward direction, and the spacecraft velocity perpendicular to the magnetic field. Figure 4 shows the orientation of the current systems from C4 (Figure 4a) and C1 and C3 (Figure 4b) mapped into the ionosphere using the *Tsyganenko and Stern* [1996] magnetic field model. Upward field-aligned currents are shown in red and downward field-aligned currents are shown in blue. In Figure 4b, the orientations from C3 are shown as dashed lines, the spacecraft ground track is shown as a dot-dashed line.

[17] The current systems observed by each of the spacecraft were consistent with field-aligned current sheets. The maximum variance direction for each of the current system was well defined ($\lambda_{max}/\lambda_{int} > 20$) and the maximum variance direction was perpendicular to the magnetic field direction. Furthermore, Figure 3 shows that the westward component of the magnetic field varied much less in each of the current regions as compared to the northward component, indicative of a current sheet structure. Data from C1 and C3 showed that the maximum variance directions of D1, U1 and U2 were close to the perpendicular northward direction (within 20°) but that D2 was tilted away from this direction (with tilts of >40°). Data from C4 showed a similar situation in D2, but also that U1 and U2 were tilted away from the perpendicular northward direction by ~30°. Similarly, the data from C1 and C3 shows that the maximum variance direction was almost perpendicular to the spacecraft velocity perpendicular to the magnetic field in U1 and U2, while the maximum variance direction in U1 and U2 observed by C4 was 30°–40° away from perpendicular to the spacecraft track. As such, we have confidence in the current densities determined by FGM on C1 and C3 in the upward current regions. Using a model of a current sheet which is infinitely long along the magnetic field direction and infinitely wide in the north-south direction, we conclude that the current densities from the FGM on C4 in the upward current regions presented in Figure 3 are underestimated by a factor ~4/3 due to the spacecraft passing

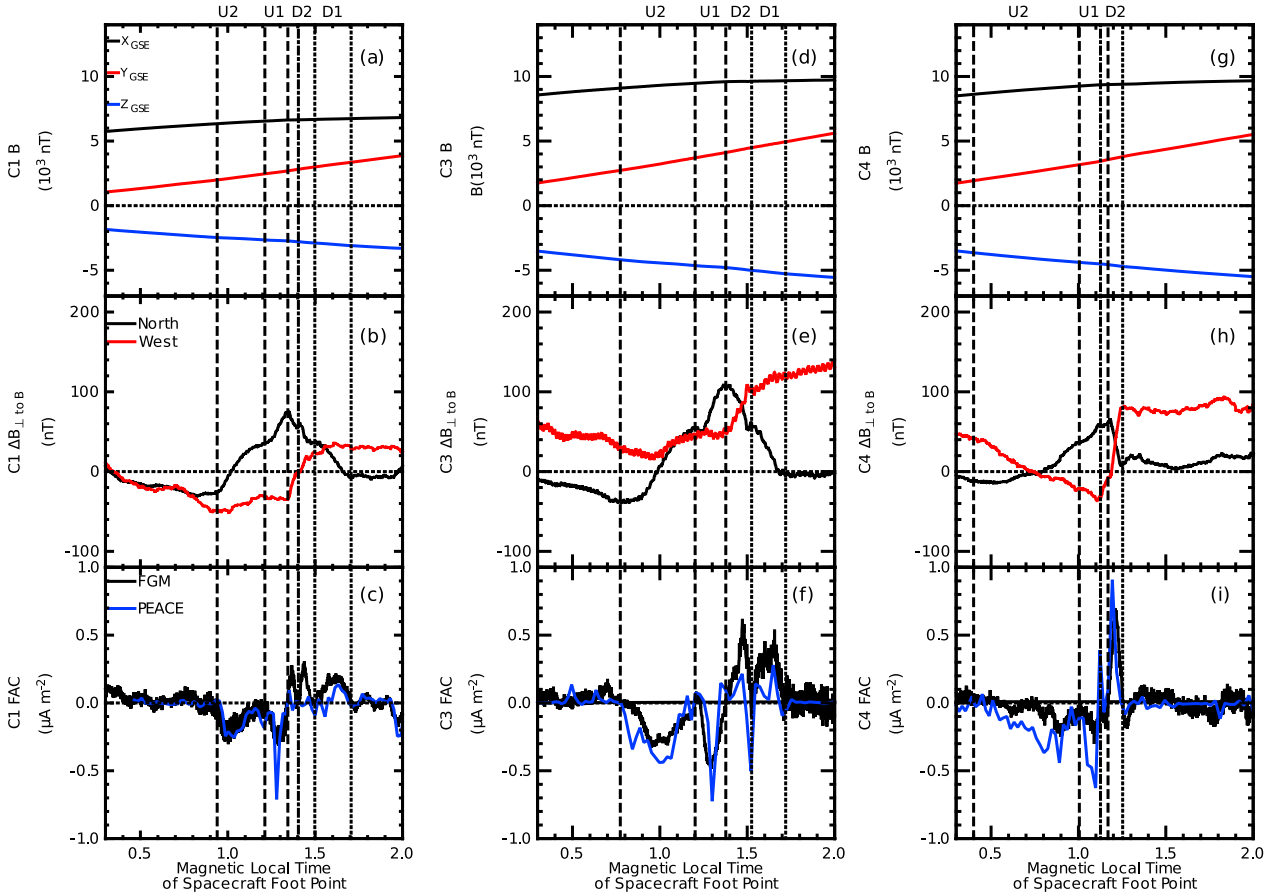

Figure 3. Data from the FGM instruments on C1, C3 and C4, plotted against MLT. (a, d, g) Traces of the magnetic field observed by C1, C3 and C4 respectively, plotted in GSE X (black), Y (red) and Z (blue) directions. (b, e, h) The residual magnetic field (FGM-T96 model), plotted in the directions northward (black) and westward (red) perpendicular to the model field from C1, C3 and C4 respectively. (c, f, i) The field-aligned current density from C1, C3 and C4 from the FGM (black) and PEACE (blue) instruments. The field-aligned currents from the FGM instruments are calculated as the gradient of the residual magnetic field perpendicular to the spacecraft track and the spacecraft velocity perpendicular to the model magnetic field. The vertical lines delimit the upward (dashed) and downward (dotted) current systems. The dot-dashed lines indicate a bifurcation of a current sheet.

Table 1. Table of the Maximum Variance Directions From MVA of the Residual Magnetic Field in the Four Current Systems Observed by Cluster[a]

	D1	D2	U1	U2
C1 Max Dir.	(–0.438, –0.032, –0.899)	(–0.525, 0.488, –0.697), (–0.494, 0.719,–0.488)	(–0.357, –0.073, –0.931)	(–0.229, –0.374, –0.899)
C1 $\lambda_{max}/\lambda_{int}$	24.24	44.83, 157.8	170.0	68.22
C3 Max Dir.	(–0.549, 0.058, –0.834)	(–0.580, 0.515, –0.632)	(–0.362, –0.155, –0.919)	(–0.245, –0.391, –0.887)
C3 $\lambda_{max}/\lambda_{int}$	35.53	40.10	37.025	48.43
C4 Max Dir.		(–0.526, 0.693, –0.493)	(–0.308, 0.932, 0.190), (–0.486, 0.399, –0.778)	(–0.447, 0.309, –0.839)
C4 $\lambda_{max}/\lambda_{int}$		750	33.80, 32.54	50.42
C1 Max - B	92.41	90.29, 89.01	89.82	90.14
C1 Max - N	9.53	41.21, 58.81	3.77	15.97
C1 Max - $V_\perp$	77.51	44.80, 26.89	81.48	100.36
C3 Max - B	93.33	90.61	88.18	88.07
C3 Max - N	17.63	45.25	1.81	16.67
C3 Max - $V_\perp$	70.64	41.88	86.39	101.49
C4 Max - B		89.93, 91.80	87.91	87.59
C4 Max - N		57.11, 101.23	33.03	25.84
C4 Max - $V_\perp$		28.76	15.85, 52.24	58.52

[a]The $\lambda_{max}/\lambda_{int}$ ratio is shown to indicate how well resolved the maximum variance direction was. Also shown are the angles between the maximum variance direction and the magnetic field direction, the perpendicular northward direction and the spacecraft velocity perpendicular to the magnetic field.

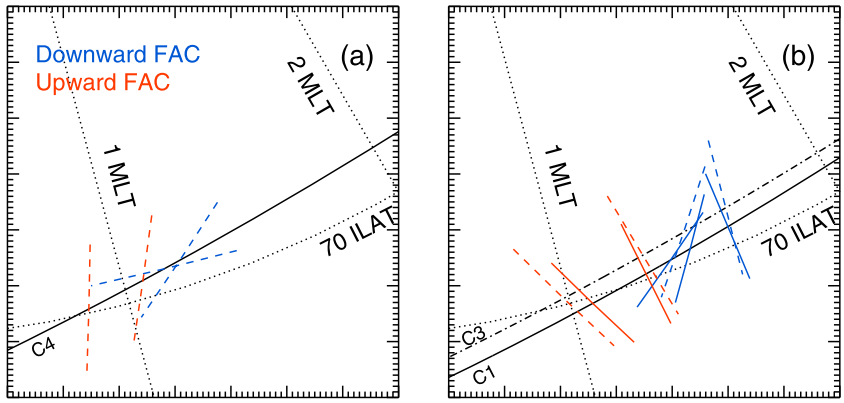

Figure 4. Plots of the orientations of the field-aligned current systems from (a) C4 and (b) C1 and C3, as determined using MVA on the residual magnetic field, mapped into the ionosphere using the *Tsyganenko and Stern* [1996] magnetic field model. The spacecraft foot points are shown as the solid (C1 and C4) or dot-dashed (C3) black lines. The upward currents are shown in red and the downward currents in blue. The currents from C3 and C4 are shown as dashed lines.

through the current sheet at an angle of 30° to the sheet normal.

[18] In the upward current region, the current densities from PEACE and FGM were well matched on C1 and C3, but the downward currents inferred from PEACE data were very much smaller (or absent) as compared to those inferred from FGM. A possible explanation is that the current-carrying upgoing electrons in the downward current region were below the low-energy cut-off of the PEACE instrument (34 eV during this event).

[19] The north-south orientation of the current sheets reported here is different to the orientation of the large scale Region 0, 1 and 2 current systems (such as observed by *Higuchi and Ohtani* [2000] and *Peria et al.* [2000]), which tend to be oriented east-west. However, small-scale structures, such as omega bands [e.g. *Opgenoorth et al.*, 1983; *Wild et al.*, 2000, 2011], can have a range of orientations; in a study of small-scale field-aligned currents by FAST [*Peria et al.*, 2000], over 6% of the small-scale field-aligned current sheets observed were orientated at more than 75° to the statistical auroral oval. Given that the FAST crossings of the auroral oval where predominantly in a north-south direction, it would preferentially detect east-west current sheets, so these observations do not fully represent the range of auroral current sheet orientations. As such, although observations of a north-south aligned current system may be uncommon, they are not unprecedented.

[20] Figure 5 shows the electric fields and electric potentials calculated from the EFW instruments on C1, C3 and C4. Figures 5a–5c show the electric field components perpendicular to the magnetic field, in the northward and westward directions. The EFW instruments measure the spin plane electric field so this coordinate rotation was performed by calculating the unmeasured component assuming $\mathbf{E}.\mathbf{B} = 0$. We note, however, that the AAR is a region in which magnetic field-aligned electric fields are expected to be present such that $\mathbf{E}.\mathbf{B} = 0$ may not be valid at all points in the AAR and hence there is some uncertainty about whether the calculated electric field component is valid at all times. Figure 5d shows the integral of the electric field along each spacecraft trajectory (C1 in black, C3 in green, C4 in blue), along with an estimate of the background potential, calculated by spline fitting the electric field data at those points at which the field-aligned current density was minimized (dashed lines) where we expect the electric potential also to be minimized. Figures 5e–5g show the potential drop below the spacecraft, calculated as the difference between the integrated electric field and the background potential. Also shown are the energies of the peaks of the upgoing ion distributions (red) and characteristic energies (total energy flux divided by total number flux, blue) of the upgoing ion distributions. No ion data are available from C3 for this event, so we have plotted the ion data from C1 in Figure 5f. C1 and C3 were approximately magnetically conjugate as they crossed the AAR but separated by ~1500 km, so we expect the potential below C3 from the EFW measurements should follow a similar trend to the ion data from C1, but with a lower amplitude.

[21] The electric field data calculated from the EFW measurements shows that the northward component of the electric field was greater than the westward component throughout the AAR crossings. This is in contrast to the observations of *Sadeghi et al.* [2011], who reported almost no variation in the northward component of the electric field during a Cluster crossing of the AAR, but consistent with the observations of *Marklund et al.* [2011a, 2011b] who reported large variations in the northward component during Cluster crossings of the AARs. In the events presented by *Sadeghi et al.* [2011], *Marklund et al.* [2001] and *Marklund et al.* [2011b], the spacecraft motion was more north-south aligned than in the case presented here. In this event, the magnetic field was inclined at less than 20° to the spin plane during the AAR crossings. As such, the northward component of the electric field presented is primarily the unmeasured component of the electric field, calculated assuming $\mathbf{E}.\mathbf{B} = 0$. As noted above, it is unclear where in the AAR this assumption is met and therefore how reliable the calculation of the northward component of the electric field is. This uncertainty could be important, given that observations from spacecraft with 3-D electric field measurements have shown that the parallel electric field in the AAR can be comparable to the perpendicular field [*Ergun et al.*, 2002]. However, because the spacecraft

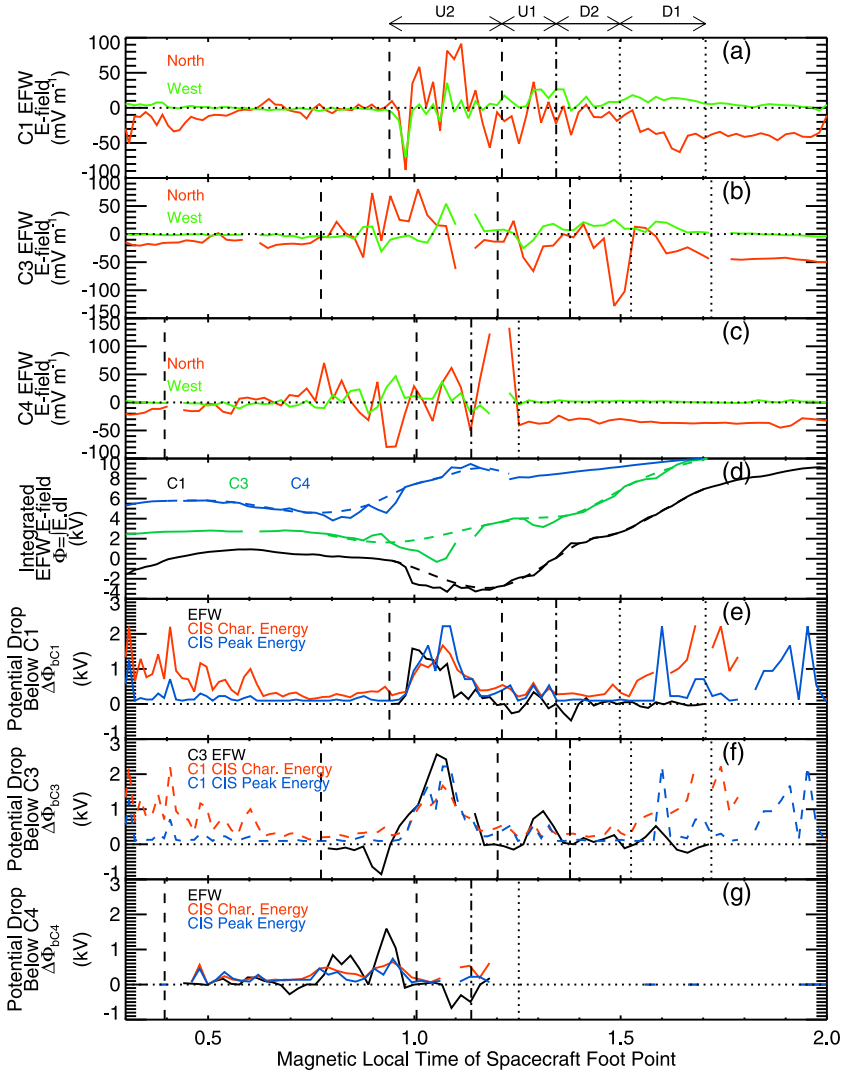

Figure 5. Plot of the electric fields and electric potentials observed by C1, C3 and C4. (a–c) Plots of the electric field measured by C1, C3 and C4 respectively in the directions northward and westward perpendicular to the magnetic field. In order that the electric field could be rotated into this coordinate system, the unmeasured component of the electric field was calculated by assuming **E**. **B** = 0. (d) Traces of the electric field integrated along the spacecraft orbits for C1 (black), C3 (green) and C4 (blue). The background potentials, calculated as a spline fit to those points at which the field-aligned current density from FGM was minimized, are plotted as dashed lines. (e–g) The electric potential drop below the spacecraft calculated from the EFW electric potential (black), ion characteristic energy (red) and peak energies of the ion phase space density spectra (blue) from C1, C3 and C4 respectively. As there is no ion data from C3, the ion data from C1, which was conjugate to but ~1500 km above, is plotted in Figure 5f. The vertical lines delimit the upward (dashed) and downward (dotted) current systems.

velocity was predominantly east-west during this event, this unmeasured component has only a small effect on the calculation of the electric potential. By comparing calculations of the AAR potentials below the spacecraft from the EFW measurements made with and without the unmeasured component, we estimate that this uncertainty is of the order of 100 V.

[22] The peak energy and characteristic energy of the field-aligned upgoing ions measured by C1 and C4 were moderately well correlated with the potential below the spacecraft from EFW between 0.6–1 MLT for C4 and between 0.9–1.3 MLT for C1 with correlation coefficients between 0.68 and 0.88 significant above the 99.9% confidence level. We expect these data to be correlated as they are both measures of the potential below the spacecraft, assuming a quasi-static potential structure [*Reiff et al.*, 1988; *McFadden et al.*, 1998, 1999]. We cannot compare the electric potential with the ion characteristic or peak energy from C3 due to the ion data being unavailable. However, the shape of the electric potential from C3 was a good match for the ion data from C1 (correlation coefficients of 0.77 and 0.57 for the characteristic and peak energies respectively, both significant to above the 99.9% confidence level), which was at higher altitude but close to conjugate to C3 throughout. It should be noted that during this event there were only two working

EFW probes on C1 and we expect the possible presence of a magnetic field-parallel electric field of unknown size, thus $\mathbf{E}.\mathbf{B} \neq 0$. This may account for the discrepancies between the EFW and CIS measurements.

[23] Across ~0.9–1.3 MLT on C1 and C3 and ~0.4–1.1 MLT on C4 we observed a potential drop below the spacecraft as expected for an upward current region (as plotted in Figure 5). However, all three spacecraft also encountered an apparent potential increase, indicating a downward pointing electric field, at various points in the AAR. In our analysis, the determination of a potential drop or potential increase below the spacecraft is highly dependent on the determination of the background potential that is removed. The data from C1 show that the variability in the potential in the region in which the potential increase was observed was small and the potential increase on C1 occurred inside a region of downward accelerated electrons, suggesting that these are less likely to be real potential increases below the spacecraft and may be a product of the calculation technique. Conversely, the potential increase below C4 occurred close to the boundary between the upward and downward current regions, is prominent in Figure 5d and coincides with ion conics. This suggests a real potential increase below the spacecraft, which will be discussed in more detail in section 5.

4. Conjugate, Multipoint Observations of the Electric Potential

[24] In order to quantitatively compare data from C1 and C3, it is necessary to determine when the spacecraft were conjugate or the spatial and temporal variations in the potential structure and incoming particle populations were negligible. We do this by directly comparing the field-aligned currents and particle spectra from the two spacecraft with respect to MLT.

[25] Liouville's Theorem states that the phase space density of an electron population accelerated by a magnetic field-aligned potential drop will be shifted in energy by the electrostatic potential energy gained through that potential drop. As such, the phase space density spectra measured by C1 and C3 should be highly correlated when the energy shift between the spacecraft is accounted for. However, given that, for Maxwellian and kappa distributions, phase space density decreases exponentially with energy, cross correlation of the electron phase space density spectra is dominated by variations in low energy plasma. As we are interested in comparing plasma populations at ~1 keV, we cross correlate the electron differential number flux spectra, which are less sensitive to variations at energies lower than are important here.

[26] Figure 6a shows the times at which the spacecraft were over each MLT, Figures 6b and 6c show the field-aligned current density per unit magnetic field from FGM and PEACE. Assuming that the current density is conserved along the magnetic field and that the separation distance perpendicular to the magnetic field shown in Figure 1 is small enough to cause no differences, these values should be equal at C1 and C3. We have compared the PEACE spectra by cross-correlating the differential number flux of the electrons at each MLT with respect to energy. Figures 6d and 6e show the square of the maximum correlation coefficient and the associated energy shift (black trace) respectively. The red trace in Figure 6d shows the general trend of the square of the correlation coefficient using a 20 s boxcar filter. The blue trace in Figure 6e shows the difference in the energies of the peaks of the electron phase space densities. This, and the energy shift from the cross-correlation analysis are measures of the potential drop between the spacecraft.

[27] The field-aligned current densities per unit magnetic field calculated from the magnetic field data were similar throughout the AAR crossing (Figures 6b and 6c). The field-aligned current densities per unit magnetic field observed by PEACE were comparable to those observed by FGM in the upward current region. Between 0.97 and 1.17 MLT, the current densities from C1 and C3 were almost identical from both FGM and PEACE. This coincides with the time at which the *Tsyganenko and Stern* [1996] model predicts that the spacecraft were closest to conjugacy (Figure 6a). The observations of the field-aligned current densities show that C1 and C3 passed through the same AAR and strongly suggest that the spacecraft were either conjugate in this AAR or that the AAR was sufficiently similar across the magnetic field that they can be considered to have sampled the same region at different heights.

[28] Figure 6d shows that the square of the maximum cross-correlation coefficient is quite variable throughout the crossing, but the general trend between 1 and 1.5 MLT is for this to be above 0.6. Between 0.97 and 1.17 MLT this variability is reduced and the square of the correlation coefficient tends to be greater than 0.6, peaking at 0.978. At this location, the current densities per unit magnetic field were identical and the spacecraft foot point separation, determined using a model magnetic field, was minimized. Also, the energy shift from the cross correlation analysis was a match for the difference in the energies of the phase space density peaks (Figure 6e). These data all indicate that C1 and C3 were effectively magnetically conjugate between 0.97 and 1.17 MLT.

[29] During the period of conjugacy, the potential drop between C1 and C3 varies between 0 V and 500 V. The potential drop between the two spacecraft dropped to 0 V twice during the period of conjugacy. This may be indicative of electric double layers containing potential drops of 300–500 V passing into and out of the region between the two spacecraft. Confirmation of this requires higher time resolution electric field data than is presented here. Due to the failure of two of the electric field probes on C1, significant additional work is required to confirm the quality of the high-time resolution electric data in the AAR thus the investigation of double layers with Cluster is beyond the scope of this paper.

[30] Using the interval of magnetic conjugacy between C1 and C3, we can examine the distribution of the electric potential drop across three distinct regions in the AAR; above C1 (the higher altitude spacecraft), between C1 and C3, and below C3 (the lower altitude spacecraft). Figure 7 shows the total potential drop seen by C1, calculated as the sum of the potential drop calculated from the ion data and the peak energy of the electron distributions on C1 (Figure 7a), the potential drop above C1 (black), between C1 and C3 (red), and below C3 (blue) (Figure 7b), and the proportion of the total potential above C1, between C1 and C3, and below C3 (Figure 7c). For consistency, the potential drop below C3 was calculated as the characteristic ion energy at C1 (the

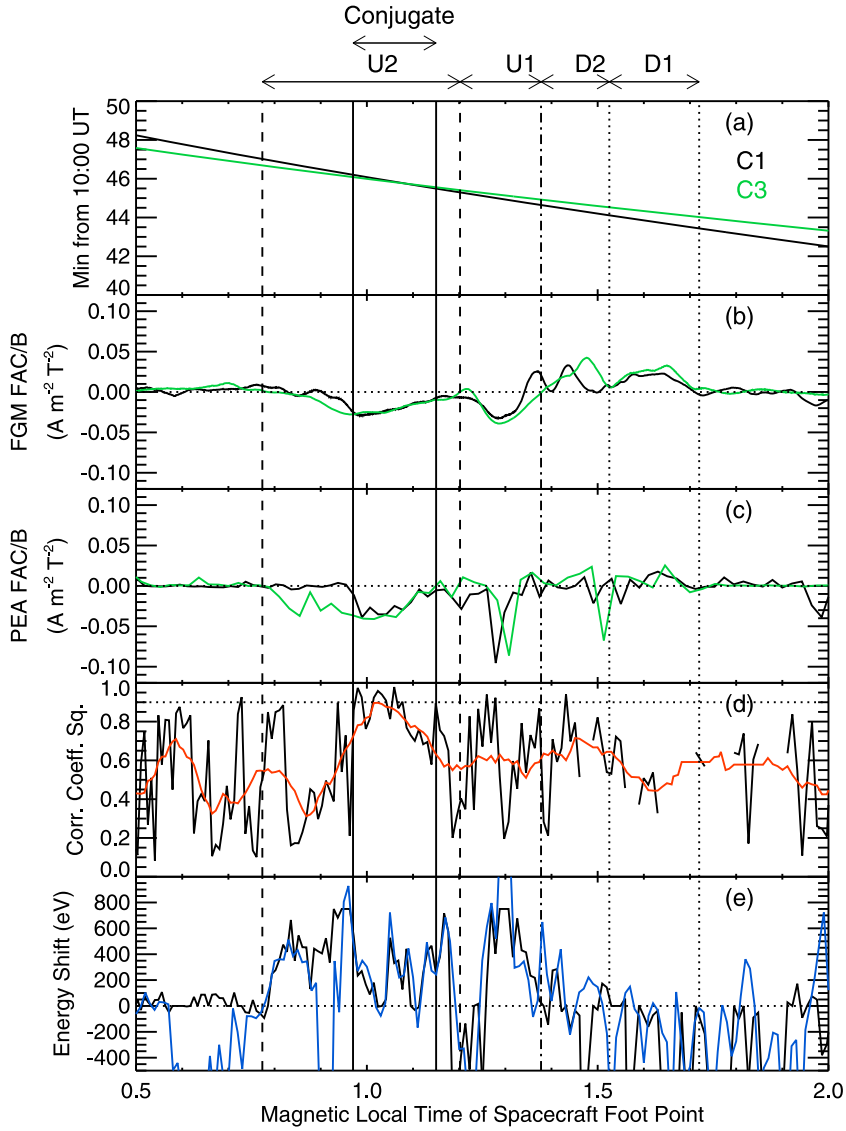

Figure 6. Plots showing the conjugacy between C3 and C4. (a) The times at which the spacecraft were over each MLT. (b and c) Field-aligned current densities per unit magnetic field from FGM (Figure 6b) and PEACE (Figure 6c) on C1 (black) and C3 (green). (d) The square of the maximum correlation coefficient from the cross-correlation of field-aligned electron differential number flux spectra from C1 and C4. (e) The energy shift of the maximum correlation coefficient (black) and the difference between the peak energies of the electron phase space density spectra. The vertical lines delimit the upward (dashed) and downward (dotted) current systems. The solid vertical lines show the region in which the spacecraft were effectively magnetically conjugate.

potential drop below C1) minus the potential drop between the C1 and C3, calculated from the cross correlation of the electron spectra at the two spacecraft. The region between the vertical solid lines in the figure shows where the spacecraft were in conjunction.

[31] The total potential drop exhibited a maximum of 2000 and 2500 V in U1 and U2 (1.28 and 1.075 MLT), respectively (Figure 7a). In U1, the potential drop was predominantly above C1 (Figure 7c). When C1 and C3 were conjugate, the potential above C1 increased steadily (spacecraft moving to lower MLTs), but made up a fairly steady proportion of the total potential drop, with a median value of 613 V (upper quartile: 951 V; lower quartile: 492 V) corresponding to 40% (upper quartile: 47%; lower quartile: 34%) of the total potential drop. Figure 7c shows that the potential drop above C1 was less than that below C3 (median value of 50% with an upper quartile of 57% and a lower quartile of 28%), and that 15% (upper quartile 25%, lower quartile 2.5%) of the potential drop was between the two spacecraft.

[32] *Marghitu et al.* [2006] developed a technique based on fitting a bi-Maxwellian distribution to the down-going electron population and using the fit parameters along with the flux of the upward going ions and total potential drop to determine the height of the top of the AAR. We have adapted this technique for use on the CIS and PEACE data from C1 to determine the height of the top of the AAR above

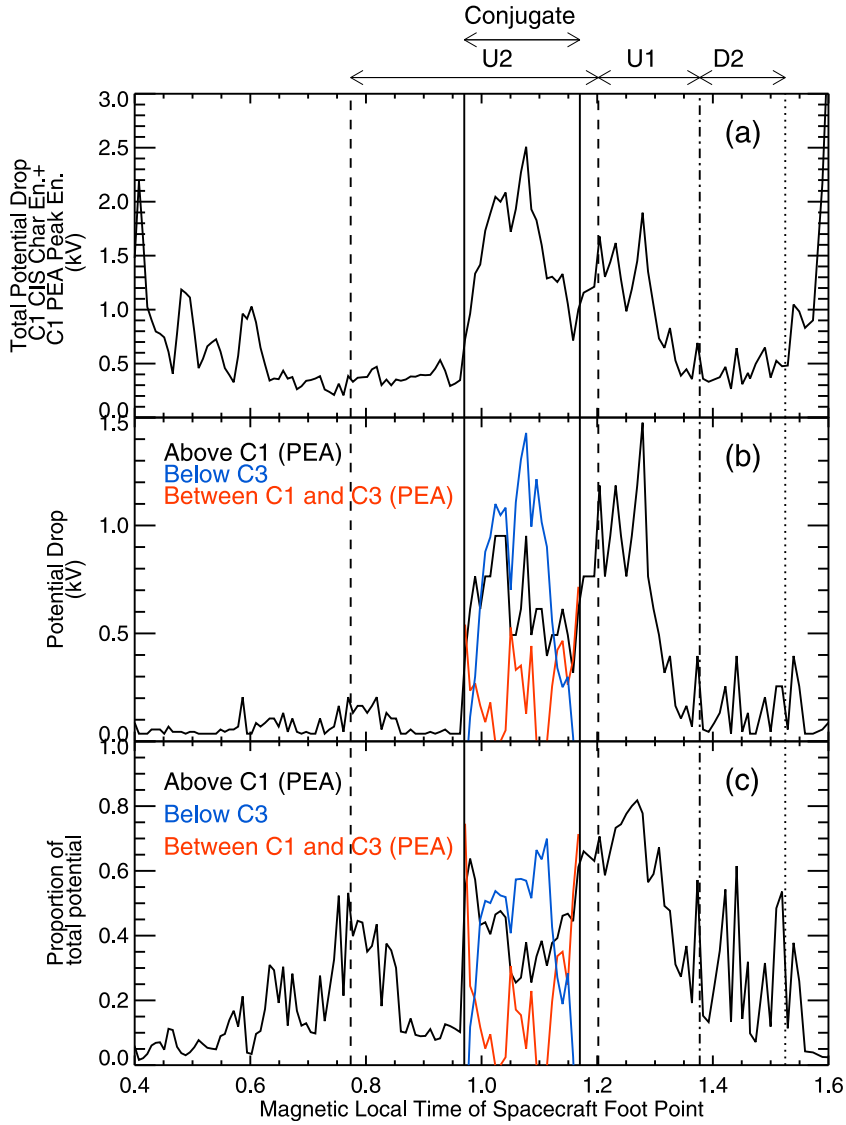

Figure 7. Plots of distribution of the total magnetic field-aligned potential drops above, below and between the spacecraft. (a) The total magnetic field-aligned potential drop, calculated as the sum of the peak electron energies and the ion characteristic energies from C1. (b) The magnetic field-aligned potential drops above C1 (black), between C1 and C3 (red) and below C3 (blue). (c) The proportion of the total magnetic field-aligned potential drop above C1 (black), between C1 and C3 (red) and below C3 (blue). The vertical lines delimit the upward (dashed) and downward (dotted) current systems. The solid vertical lines show the region in which the spacecraft were effectively magnetically conjugate.

C1 (see Appendix A). Figure 8a shows the χ^2 per number of energy bins ($\langle\chi^2\rangle$) for the fit of the electron distribution function to the model function in the magnetic field-parallel (black) and perpendicular (red) directions, indicative of the goodness-of-fit of the model. Figure 8b shows the altitude of the top of the AAR calculated at those points where $\langle\chi^2\rangle$ <20 from both the parallel and perpendicular fits. The dotted line indicates a distance of 2 R_E for reference.

[33] Using the calculated height of the top of the AAR and the altitudinal separation of C1 and C3, we can determine the spatially averaged electric field across the AAR above and between the spacecraft. These are shown in Figure 8c. The top of the AAR was between 3100 km and 7100 km above C1 when the C1 and C3 were conjugate and the $\langle\chi^2\rangle$ values suggest that the model fit to the distributions was good, with values generally less than 10 for the perpendicular spectra and less than 1 for the parallel spectra. The spatially averaged electric field above C1 varied between 0.04 mV/m and 0.3 mV/m whereas the spatially averaged electric field between the spacecraft varied between 0 mV/m and 0.47 mV/m. These electric field values are less than half those determined by *Sadeghi et al.* [2011] for the average electric field inside the AAR in their event.

[34] The *Marghitu et al.* [2006] technique assumes that the source population is Maxwellian. From a small number of case studies in which the Polar and FAST satellites were conjugate, *Janhunen et al.* [2001] suggested that the source particle populations were non-Maxwellian in AARs in which

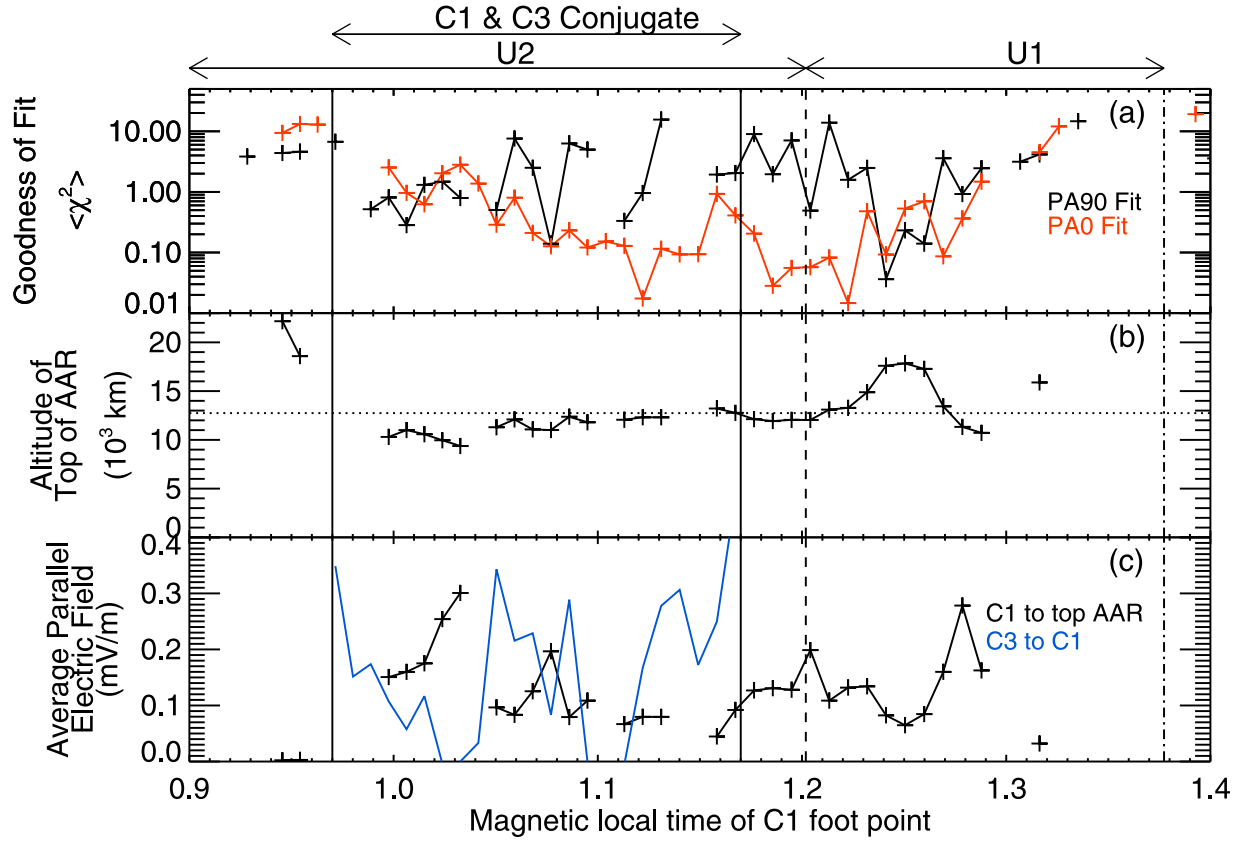

Figure 8. Plots of the distance between C1 and the top of the AAR, based on the technique of *Marghitu et al.* [2006], and the average electric fields above C1 and between C1 and C3. (a) The χ^2 value per energy bin for the fits of the model electron distribution to the measured distributions in the parallel (black) and perpendicular (red) directions. (b) The altitude of the top of the AAR calculated using the technique of *Marghitu et al.* [2006]. The dashed line indicates a height of 2 R_E. (c) The average electric field between C1 and the top of the AAR (black) and between C1 and C3 (blue). The vertical lines delimit the upward (dashed) and downward (dotted) current systems. The solid vertical lines show the region in which the spacecraft were effectively magnetically conjugate.

the total accelerating potential was large (>2 kV). In their study, the low altitude electron distributions could be explained by a U-shaped potential drop accelerating the high-altitude Maxwellian distribution, but not the non-Maxwellian distributions. The total potential drop in our event is close to the limit at which *Janhunen et al.* [2001] expect to stop seeing a Maxwellian source population, with our total potential drop peaking above 2 kV but the majority of the potential drop below 2 kV. The relatively good fit of the data to model Maxwellians (Figure 8a) and the strong cross-correlation between the spectra of the down-going electrons (Figure 6d) suggest that the source was sufficiently Maxwellian that the *Marghitu et al.* [2006] technique is appropriate.

5. Differences in the AAR Observed by C3 and C4

[35] During this event, C3 and C4 were on the same orbit track separated by 192 s, although their observations of the AAR were separated by only 150 s, suggesting that the AAR moved between the crossings. In this section, we analyze the differences between these two spacecraft crossings and present an interpretation of these differences in terms of the temporal evolution of the electrostatic potential drop by assuming a spatial invariance in the potential structure along its length.

[36] Figure 9 shows the field-aligned current densities from FGM and the potential drops above and below C3 (green) and C4 (blue), determined from the peak of the electron phase space densities and the integrated electric field respectively. The blue dashed line in Figure 9c shows the potential below C4 from the ion characteristic energy. The black line in Figure 9c shows the potential below C3 calculated as the potential below C1 from the ion characteristic energy less the potential difference between C1 and C3 from the peaks of the electron phase space density when these spacecraft were conjugate (see section 4). The data from Cluster 4 have been shifted by 0.21 MLT to bring them into alignment with the data from C3. The field-aligned current densities calculated from FGM on C4 have been multiplied by 4/3 to correct for the upward current sheets being tilted at an angle of ~30° to the spacecraft path. Examining the field-aligned current densities and potential drops above the spacecraft from C4 suggests that rather than a single upward current region, U2 consisted of two upward current regions (hereafter U2a and U2b). These are split by the dotted vertical line at 1.08 MLT

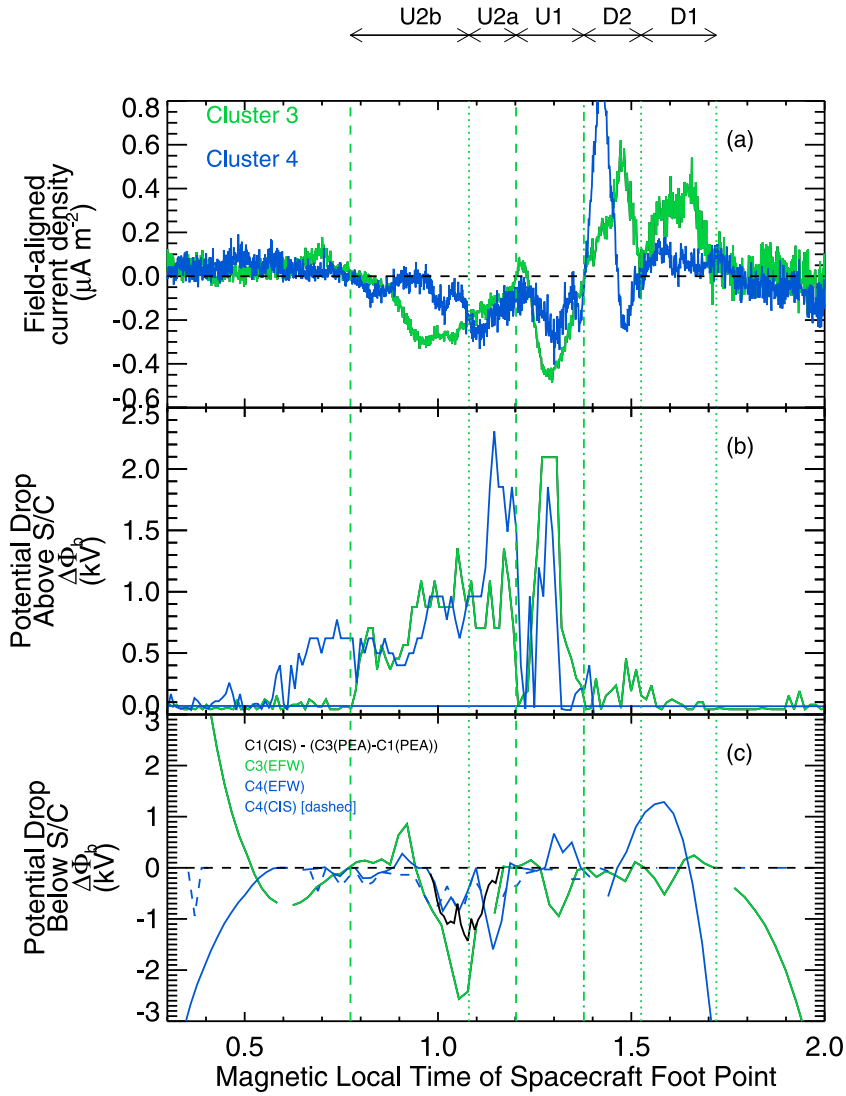

Figure 9. Plots of (a) the field-aligned current density, (b) the potential above C3 and C4 and (c) the potential below C3 and C4. Data from C3 is shown in green, data from C4 is shown in blue. The black line in Figure 9c shows the potential below C3 calculated as the potential below C1 from the ion characteristic energy less the potential difference between the spacecraft from the electron phase space density peaks (see section 4). The blue dashed line shows the potential drop below C4 from the CIS-CODIF data. The vertical lines delimit the upward (dashed) and downward (dotted) current systems from C4.

in Figure 9. The field-aligned currents at C3 show that U2 was a single current system.

[37] Between the crossings by C4 and C3, the AARs were somewhat similar, in particular showing similar potential drops above C3 and C4, but had moved eastward by 0.21 hours MLT. There were, however, some notable differences. The FGM magnetic field data show an additional downward current region was observed by C3 at the eastward side of the AAR. The current density in U1 and U2b was 0.15–0.3 μA m^{-2} higher during the C3 crossing, whereas in U2a the current density was <0.05 uA m^{-2} lower during the C3 crossing. In U1, the potential drop above the spacecraft was ~250 V lower during the C3 crossing, but we note that this is equivalent to the energy resolution of the data at 2000 eV. As such, the difference in the potential drop above the spacecraft in U1 may have been somewhat smaller. Data from the EFW instrument on C4 indicates that there was a downward pointing parallel electric field below the spacecraft, whereas there was an upward pointing electric field below C3. The potential difference below C3 was reversed compared to C4 and changed by 1.7 kV.

[38] In the classic model of quasi-static potential drops [e.g. *Lyons*, 1980; *Temerin et al.*, 1981], the potential contours have U-shapes such that a spacecraft sampling electric fields above the potential drop region should detect a decrease followed by a increase in the potential. As C4 passed from D2 to U1 it observed an increase in potential below the spacecraft followed by an decrease. At the same time, C4 observed downgoing electrons and ion conics (Figure 2). These observations all indicate that during C4's passage through the upward current region U1 there was a region of upward electric field above the spacecraft and downward electric

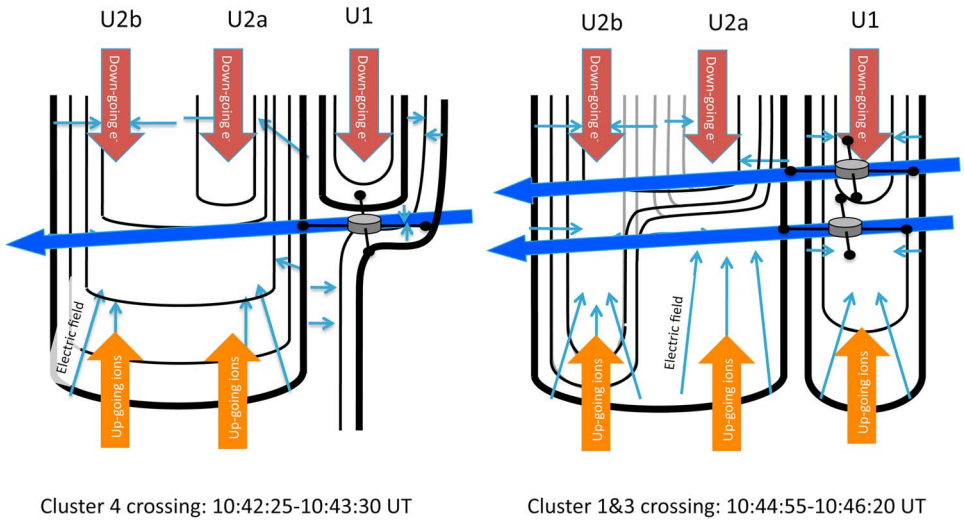

Figure 10. A schematic of the electric potential structure of the AAR based on the observations presented. The diagram on the left shows the potential structure during the C4 crossing and the diagram on the right shows the structure during the C1 and C3 crossings. The black lines indicate electric potential contours in arbitrary potential steps, with the thick lines indicating 0 V. The light blue arrows indicate the electric field. The grey lines indicate the potential structure observed by C3 and highlight the differences between the C3 and C1 data. The presence of upgoing ions and down-going electrons is indicated by the orange and red arrows respectively. The spacecraft path through the AAR is indicated by the blue arrow.

field below or in the vicinity of the spacecraft. This structure could consist of a U-shaped potential at high altitude bracketed by an S-shaped potential at lower altitude. Such a situation was observed by *Marklund et al.* [2011b], although with an upward electric field in the S-shaped structure. In the upward current region U2, C4 made observations more typical of the classic model of auroral potential drops. C3 observed potential drops below the spacecraft in U1, U2a and U2b indicating classic U-shaped structures. This is consistent with the observations of upgoing ions in both U1 and U2 observed by C1 at higher altitude.

[39] Our observations of the magnetic field and particle signatures show that the upward current regions investigated here rotated and moved between the spacecraft crossings (Figure 4). Furthermore, the near north-south, rather than east-west, alignment of the current sheets may suggest that these current systems cannot be treated as "infinitely" long current sheets which are invariant along there length, although the magnetic field data strongly indicates that the upward current regions are long current sheets. As such, it is unclear whether the differences described above are due to the spacecraft passing through different sections of the upward current regions, temporal variations in the structure of the region or some combination of these factors, although the data are sufficiently similar to suggest that both spacecraft passed through the same upward current regions. From the observations presented, we cannot determine any motion of the AAR perpendicular to the spacecraft track, we choose to analyze these observations in terms of a purely temporal evolution of the structure. This analysis assumes that the structure is sufficiently invariant along its length so as to negate any spatial variability in the structure. This analysis is also highly dependent on our assumption that the various current systems identified in the C3 and C4 data are the same.

[40] The observations from C3 and C4 show that large differences in the field-aligned currents appear to be associated with differences in the potential drop below ~4000 km. Assuming that these changes are temporal, the relationship between the change in the current density and the change in the potential drop is different in each current sheet, suggesting that the current systems change size or that the conductivity along each individual current system is somewhat different.

[41] Under the assumptions above, we calculate the average rate of change of the current density and potential by dividing the change in these quantities by the interval between the crossings. Comparing the current densities in U1 and U2b, we calculate an average rate of increase in the current density of 1–2 nA m^{-2} s^{-1} and an average rate of decrease in the current density in U2a of <0.3 nA m^{-2} s^{-1}. Similarly, in U1 and U2b the potential below the spacecraft increased at an average rate of 6.6 V s^{-1} using the particle measurements (black and dashed blue lines) or 11 V s^{-1} using the electric field measurements.

6. Summary of Observations

[42] Figure 10 presents a schematic view of the electric potential structure in the AARs encountered by Cluster based on the observations in the upward current sheets U1, U2a and U2b. The black lines show the potential structure observed by C1 and C4 and the grey lines show the structure observed by C3. Thick lines indicate a potential of 0 V. The spacecraft path through the AAR and observations of upgoing ions and down-going electrons are indicated by the colored arrows and the direction of the electric field is shown by the light blue arrows.

[43] From C3 and C4, which were on the same orbit but separated in time, we observed that the potential structure

moved eastward between the two crossings by 0.21 MLT. The observations show that the field-aligned current density was higher during the second spacecraft crossing in U1 and U2b, but lower in U2a. Similarly, the potential difference below the spacecraft was greater during the second spacecraft crossing in U1 and U2b. In U2a, the field-aligned current density and potential difference below the spacecraft was slightly lower during the second spacecraft crossing, but the potential drop above the spacecraft was the same between the two crossings.

[44] C1 and C3 effectively came into magnetic conjugacy during the crossing, as shown by their near-identical field-aligned current densities per unit magnetic field and the strong cross-correlation of the down-going electron spectra. We observed that the potential drop inside the AAR between the two spacecraft varied between 0 V and 500 V, ~15% of the total potential drop across the AAR. The majority (>50%) of the potential drop was concentrated below C3 (~4600 km altitude) and the top of the AAR was ~1 R_E above C1, which was at 6235 km altitude.

7. Discussion

[45] Multipoint observations offer a unique opportunity to study the spatial structure and temporal variability of the AAR. In the event presented here, we have studied both of these aspects. We have shown that, for two neighboring upward current regions, the vertical distribution of the parallel potential drop was quite different; the potential drop was concentrated at low altitudes for one of the current system and at high altitudes for the other. We have also shown that the increases in the current density are associated with increases in the potential drop below the spacecraft rather than a uniform increase in the potential drop with altitude.

[46] The current systems presented in this study are small compared to the global Region 0, 1 and 2 currents that define the auroral regions. The combined upward and downward current regions covered less than 1 MLT which corresponds to 560 km in the ionosphere at 70° ILAT, with the upward current regions covering between 80 km and 340 km in MLT and the structures appeared to move eastward at 0.8 km s^{-1}. These scale sizes and eastward motion, along with the apparent rotation of the upward current sheets, are consistent with previous observations of auroral omega bands [*Opgenoorth et al.*, 1983; *Wild et al.*, 2000, 2011]. These features are commonly seen toward the end of a substorm and our observations are consistent with this. Such a structure might also explain why Cluster 3 observed a dropout in the down-going electron flux at 1.2 MLT but C1 did not, with C3 passing into the dark region in the middle of an auroral band and C1 skimming through the edge of the bright band itself. However, the lack of suitable auroral images during our event means that we cannot confirm what auroral forms were associated with the signatures observed by Cluster.

[47] Recent observations of the upward current region have shown that on the dayside the AAR can remain temporally invariant over 5 min [*Marklund et al.*, 2011a]. *Sadeghi et al.* [2011] studied two nightside upward current regions crossed by Cluster in a case where three of the spacecraft passed through the same AAR one after another. During the *Sadeghi et al.* [2011] event, the Cluster spacecraft crossed the AAR at an altitude of 1–1.5 R_E, higher than the event we present here. Similar to our analysis, *Sadeghi et al.* [2011] interpreted the differences in the potential structure between the spacecraft crossings as as a temporal change in the AAR, with the potential below the spacecraft increasing by 2 kV during the 100 s between the first and last spacecraft crossings in one of the AARs the potential increased over the 100 s between the first and last crossing, while the potential drop above the spacecraft was relatively invariant. However, unlike the event presented here, the orientation of the current sheets in their event was east-west aligned.

[48] Taking the results of *Sadeghi et al.* [2011] and those presented in this paper as showing a temporal evolution of the AAR, it is unclear what physical parameters control this evolution. Our observations suggest that in both upward current regions, the potential above the height of C3 and C4 was almost unchanged, but the current density and potential drop below the spacecraft increased, with average rates of change of 0.3–2 *nA* m^{-2} s^{-1} and ~6–11 V s^{-1}, respectively. This is somewhat slower than the average rates of change from *Sadeghi et al.* [2011], which we calculate to be 37.5–50 V s^{-1} with negligible change in the current density. It remains a challenge for theorists and modelers to reproduce this temporal variability, while further multispacecraft observations of the kind presented here are needed to understand how common this increase in the low-altitude potential in conjunction with an increase in the field-aligned current density is.

[49] Models of the vertical structure of the AAR [*Ergun et al.*, 2000] have indicated the presence of static double layers at the limits of the region, acting to separate the high-density ionosphere, low density auroral cavity and intermediate-density magnetosphere. Double layers have also been observed within the AAR by FAST [*Ergun et al.*, 2004], although this single spacecraft was unable to determine whether the double layers were stationary structures or moving along the magnetic field. *Pottelette et al.* [2003] suggested that double layers moving through the AAR could be responsible for creating plasma distributions capable of generating AKR, with their vertical motion responsible for the increasing frequency of the fine structure. The observations presented here show that there were times where the potential difference between C1 and C3 was near 0 V. This may be due to the energy resolution of the PEACE instrument, such that the instruments were unable to resolve a potential difference less than ~100 V for 1000 eV electrons. If these measurements are of a real effect, it may be that these periods of high or no-potential-drop between the spacecraft might also be explained by double layers passing into and out of the region between the spacecraft. We note that the electric field data were highly variable during this event, consistent with a picture where the acceleration of electrons and ions took place in localized potential drops rather than a smoothly varying potential drop across the AAR. A further study, examining the electron distributions perpendicular to the magnetic field and the high-time-resolution electric field data, will be undertaken to examine the possibility of identifying double layers in the AAR with Cluster.

8. Summary

[50] In this study, we have examined the auroral acceleration region using multipoint data from the Cluster spacecraft when two of the spacecraft (C3 and C4) were on the

same orbit but separated by 192 s and two of the spacecraft (C1 and C3) approached magnetic conjugacy, separated by 1500 km along the magnetic field. The spacecraft passed through a region of downward field-aligned current, then two regions of upward field-aligned current and observed the associated flux of ionospheric ions flowing upward along the magnetic field and magnetospheric electrons flowing downward along the magnetic field. Multipoint observations of the upward current AAR using two spacecraft on the same orbit but separated in time show that the upward current sheets rotated and moved between the two crossings. Due to the limited observations along the current sheet length, we interpreted these observations as an evolution of the quasi-static potential structure assuming that the structure had sufficient spatial invariance to make any cross-track variations negligible. We have shown that:

[51] 1. the overall structure of the AAR was fairly steady on a timescale of 150 s, but the two neighboring upward current regions showed different detailed evolution,

[52] 2. the potential difference below the spacecraft differed by 1–1.7 kV in the C3 crossing compared to the C4 crossing, giving an average rate of change in the potential of $\sim$11 V s^{-1} under the above assumptions,

[53] 3. the field-aligned current density during the C3 crossing was 0.15–3 μA m^{-2} higher in two parts of the AAR and 0.05 μA m^{-2} lower in another part of the AAR compared to the C4 crossing, giving average rates of change of 0.3–2 nA m^{-2} s^{-1} under the above assumptions,

[54] 4. the potential drop above the spacecraft was almost the same in both crossings.

[55] By comparing the field-aligned current density per unit magnetic field and cross-correlating the electron spectra from two spacecraft passing through the AAR at different altitudes, we were able to determine that the spacecraft were effectively conjugate during the AAR crossing. Our results are the first such conjugate observations, with two spacecraft separated by 1500 km inside the AAR. From these observations we were able to show that:

[56] 1. the potential drop was concentrated below 4685 km.

[57] 2. on average, 15% of the potential drop was seen between C1 and C3 at 4685–6235 km altitude,

[58] 3. the average electric field between C1 and C3 was higher than the average electric field above the spacecraft [determined from the potential drop above the spacecraft and the height of the top of the AAR, calculated using the technique of] [*Marghitu et al.*, 2006], suggesting that the change in the potential drop decreases with altitude.

[59] These observations add to the growing number of multipoint studies of the AAR using closely separated spacecraft which are helping us to move to a more dynamic picture of auroral acceleration in keeping with the observed dynamics of the aurora.

Appendix A

[60] By assuming that a Maxwellian source distribution of electrons was accelerated along the magnetic field by an electrostatic potential drop, *Marghitu et al.* [2006, equation (4)] showed that the electron distribution function can be described in terms of the energy, density and anisotropy of the electrons;

$$f_M = K \times \frac{n_S}{A_s W_{0_{\|}S}^{3/2}} \times \exp\left[-\left(\frac{W_{\|M} - W_A}{W_{0_{\|}S}} + \frac{W_{\perp M}}{A_M W_{0_{\|}S}}\right)\right], \quad \text{(A1)}$$

where f is the distribution function, $K = (m/2\pi)^{3/2}$, n is the electron density, W is the energy, W_0 is the temperature and W_A is the energy gained through the accelerating potential drop. Subscript M indicates a measurement at the spacecraft location and subscript S indicates a value at the source (top of the potential drop). *Marghitu et al.* [2006] fit this function to the 2-D pitch angle data from FAST to determine n_S/A_S and A_M, which can then be used to determine the height of the top of the AAR [*Marghitu et al.* 2006, equations (12) and (13)].

[61] In this study we simplify the technique by fitting the parallel and perpendicular components of the distribution individually using the MPFIT [*Markwardt*, 2009] routines in IDL. These return the χ^2 value for the fit of both the parallel and perpendicular distribution functions. Similar to [*Marghitu et al.*, 2006], we use the reduced χ^2 to determine the goodness-of-fit, however rather than comparing a single value we compare the values from both directions.

[62] **Acknowledgments.** C.F., A.N.F., A.P.W. and C.J.O. were funded by STFC grant ST/H00260X/1. C.E.J.W. was supported by the Canadian Space Agency. We thank the CAA and Cluster instrument teams for providing the data for this study.

[63] Robert Lysak thanks the reviewers for their assistance in evaluating this paper.

References

Balogh, A., et al. (2001), The Cluster Magnetic Field Investigation: Overview of in-flight performance and initial results, *Ann. Geophys.*, *19*, 1207–1217.

Block, L. P. (1972), Potential double layers in the ionosphere, *Cosmic Electrodyn.*, *3*, 349–376.

Carlqvist, P., and R. Boström (1970), Space-charge regions above the aurora, *J. Geophys. Res.*, *75*, 7140–7146, doi:10.1029/JA075i034p07140.

Chaston, C. C., C. W. Carlson, J. P. McFadden, R. E. Ergun, and R. J. Strangeway (2007), How important are dispersive Alfvén waves for auroral particle acceleration?, *Geophys. Res. Lett.*, *34*, L07101, doi:10.1029/2006GL029144.

Dunlop, M. W., D. J. Southwood, K.-H. Glassmeier, and F. M. Neubauer (1988), Analysis of multipoint magnetometer data, *Adv. Space Res.*, *8*, 273–277, doi:10.1016/0273-1177(88)90141-X.

Ergun, R. E., C. W. Carlson, J. P. McFadden, F. S. Mozer, and R. J. Strangeway (2000), Parallel electric fields in discrete arcs, *Geophys. Res. Lett.*, *27*, 4053–4056, doi:10.1029/2000GL003819.

Ergun, R. E., L. Andersson, D. S. Main, Y. Su, C. W. Carlson, J. P. McFadden, and F. S. Mozer (2002), Parallel electric fields in the upward current region of the aurora: Indirect and direct observations, *Physics of Plasmas*, *9*, 3685–3694, doi:10.1063/1.1499120.

Ergun, R. E., et al. (2004), Auroral particle acceleration by strong double layers: The upward current region, *J. Geophys. Res.*, *109*, A12220, doi:10.1029/2004JA010545.

Fazakerley, A. N., A. D. Lahiff, I. Rozum, D. Kataria, H. Bacai, C. Anekallu, M. West, and A. Åsnes (2010), Cluster-PEACE In-flight Calibration Status, in *The Cluster Active Archive, Studying the Earth's Space Plasma Environment*, edited by H. Laakso, M. Taylor, and C. P. Escoubet, pp. 281–299, Springer, Dordrecht, Netherlands, doi:10.1007/978-90-481-3499-119.

Forsyth, C., M. Lester, A. N. Fazakerley, C. J. Owen, and A. P. Walsh (2011), On the effect of line current width and relative position on the multi-spacecraft curlometer technique, *Planet. Space Sci.*, *59*, 598–605, doi:10.1016/j.pss.2009.12.007.

Frank, L. A., and K. L. Ackerson (1971), Observations of charged particle precipitations into the auroral zone, *J. Geophys. Res.*, *76*, 3612–3643, doi:10.1029/JA076i016p03612.

Goertz, C. K., and R. W. Boswell (1979), Magnetosphere-ionosphere coupling, *J. Geophys. Res.*, *84*, 7239–7246, doi:10.1029/JA084iA12p07239.

Gustafsson, G., et al. (2001), First results of electric field and density observations by Cluster EFW based on initial months of operation, *Ann. Geophys.*, *19*, 1219–1240.

Hasegawa, A. (1976), Particle acceleration by MHD surface wave and formation of aurora, *J. Geophys. Res.*, *81*, 5083–5090, doi:10.1029/JA081i028p05083.

Higuchi, T., and S. Ohtani (2000), Automatic identification of large-scale field-aligned current structures and its application to night-side current systems, in *Magnetospheric Current Systems*, *Geophys. Monogr. Ser.*, vol. 118, edited by S.-I. Ohtani et al., pp. 389–394, AGU, Washington, D. C.

Hull, A. J., J. W. Bonnell, F. S. Mozer, and J. D. Scudder (2003), A statistical study of large-amplitude parallel electric fields in the upward current region of the auroral acceleration region, *J. Geophys. Res.*, *108*(A1), 1007, doi:10.1029/2001JA007540.

Janhunen, P., A. Olsson, W. K. Peterson, H. Laakso, J. S. Pickett, T. I. Pulkkinen, and C. T. Russell (2001), A study of inverted-V auroral acceleration mechanisms using Polar/Fast Auroral Snapshot conjunctions, *J. Geophys. Res.*, *106*, 18,995–19,012, doi:10.1029/2001JA900012.

Johnstone, A. D., et al. (1997), PEACE: A Plasma Electron and Current Experiment, *Space Sci. Rev.*, *79*, 351–398.

Keiling, A., J. R. Wygant, C. Cattell, W. Peria, G. Parks, M. Temerin, F. S. Mozer, C. T. Russell, and C. A. Kletzing (2002), Correlation of Alfvén wave Poynting flux in the plasma sheet at 4–7 R_E with ionospheric electron energy flux, *J. Geophys. Res.*, *107*(A7), 1132, doi:10.1029/2001JA900140.

Khotyaintsev, Y., P.-A. Lindqvist, A. Eriksson, and M. André (2010), The EFW data in the CAA, in *The Cluster Active Archive: Studying the Earth's Space Plasma Environment*, edited by H. Laakso, M. Taylor, and C. P. Escoubet, pp. 97–108, Springer, Dordrecht, Netherlands, doi:10.1007/978-90-481-3499-16.

Lindqvist, P.-A., and G. T. Marklund (1990), A statistical study of high-altitude electric fields measured on the Viking satellite, *J. Geophys. Res.*, *95*, 5867–5876, doi:10.1029/JA095iA05p05867.

Lu, G., P. H. Reiff, T. E. Moore, and R. A. Heelis (1992), Upflowing ionospheric ions in the auroral region, *J. Geophys. Res.*, *97*(A11), 16,855–16,863, doi:10.1029/92JA01435.

Lyons, L. R. (1980), Generation of large-scale regions of auroral currents, electric potentials, and precipitation by the divergence of the convection electric field, *J. Geophys. Res.*, *85*(A1), 17–24, doi:10.1029/JA085iA01p00017.

Lyons, L. R., D. S. Evans, and R. Lundin (1979), An observed relation between magnetic field-aligned electric fields and downward electron energy fluxes in the vicinity of auroral forms, *J. Geophys. Res.*, *84*(A2), 457–461, doi:10.1029/JA084iA02p00457.

Lysak, R. L., and C. W. Carlson (1981), The effect of microscopic turbulence on magnetosphere-ionosphere coupling, *Geophys. Res. Lett.*, *8*(3), 269–272, doi:10.1029/GL008i003p00269.

Lysak, R. L., and C. T. Dum (1983), Dynamics of magnetosphere-ionosphere coupling including turbulent transport, *J. Geophys. Res.*, *88*(A1), 365–380, doi:10.1029/JA088iA01p00365.

Marchaudon, A., J.-C. Cerisier, J.-M. Bosqued, C. J. Owen, A. N. Fazakerley, and A. D. Lahiff (2006), On the structure of field-aligned currents in the mid-altitude cusp, *Ann. Geophys.*, *24*, 3391–3401, doi:10.5194/angeo-24-3391-2006.

Marghitu, O., B. Klecker, and J. P. McFadden (2006), The anisotropy of precipitating auroral electrons: A FAST case study, *Adv. Space Res.*, *38*, 1694–1701, doi:10.1016/j.asr.2006.03.028.

Marklund, G. T., et al. (2001), Temporal evolution of the electric field accelerating electrons away from the auroral ionosphere, *Nature*, *414*, 724–727.

Marklund, G. T., S. Sadeghi, T. Karlsson, P.-A. Lindqvist, H. Nilsson, C. Forsyth, A. Fazakerley, E. A. Lucek, and J. Pickett (2011a), Altitude distribution of the auroral acceleration potential determined from Cluster satellite data at different heights, *Phys. Rev. Lett.*, *106*, 055002, doi:10.1103/PhysRevLett.106.055002.

Marklund, G. T., et al. (2011b), Evolution in space and time of the quasi-static acceleration potential of inverted-V aurora and its interaction with Alfvénic boundary processes, *J. Geophys. Res.*, *116*, A00K13, doi:10.1029/2011JA016537.

Markwardt, C. B. (2009), Non-linear least-squares fitting in IDL with MPFIT, in *Astronomical Data Analysis Software and Systems XVIII*, *ASP Conf. Ser.*, vol. 411, edited by D. A. Bohlender, D. Durand, and P. Dowler, pp. 251–254, Astron. Soc. of the Pac., San Francisco, Calif.

McFadden, J. P., et al. (1998), Spatial structure and gradients of ion beams observed by FAST, *Geophys. Res. Lett.*, *25*, 2021–2024, doi:10.1029/98GL00648.

McFadden, J. P., C. W. Carlson, R. E. Ergun, D. M. Klumpar, and E. Moebius (1999), Ion and electron characteristics in auroral density cavities associated with ion beams: No evidence for cold ionospheric plasma, *J. Geophys. Res.*, *104*, 14,671–14,682, doi:10.1029/1999JA900035.

McIlwain, C. E. (1960), Direct measurement of particles producing visible auroras, *J. Geophys. Res.*, *65*(9), 2727–2747, doi:10.1029/JZ065i009p02727.

Mozer, F. S., and A. Hull (2001), Origin and geometry of upward parallel electric fields in the auroral acceleration region, *J. Geophys. Res.*, *106*, 5763–5778, doi:10.1029/2000JA900117.

Mozer, F. S., and C. A. Kletzing (1998), Direct observation of large, quasi-static, parallel electric fields in the auroral acceleration region, *Geophys. Res. Lett.*, *25*(10), 1629–1632, doi:10.1029/98GL00849.

Mozer, F. S., C. W. Carlson, M. K. Hudson, R. B. Torbert, B. Parady, J. Yatteau, and M. C. Kelley (1977), Observations of paired electrostatic shocks in the polar magnetosphere, *Phys. Rev. Lett.*, *38*, 292–295, doi:10.1103/PhysRevLett.38.292.

Mozer, F. S., C. A. Cattell, M. K. Hudson, R. L. Lysak, M. Temerin, and R. B. Torbert (1980), Satellite measurements and theories of low altitude auroral particle acceleration, *Space Sci. Rev.*, *27*, 155–213, doi:10.1007/BF00212238.

Olsson, A., and P. Janhunen (2003), Some recent developments in understanding auroral electron acceleration processes, *IEEE Trans. Plasma Sci.*, *31*, 1178–1191, doi:10.1109/TPS.2003.821352.

Opgenoorth, H. J., J. Oksman, K. U. Kaila, E. Nielsen, and W. Baumjohann (1983), Characteristics of eastward drifting omega bands in the morning sector of the auroral oval, *J. Geophys. Res.*, *88*(A11), 9171–9185, doi:10.1029/JA088iA11p09171.

Paschmann, G., S. Haaland, and R. Treumann (Eds.) (2003), *Auroral Plasma Physics*, ISSI/ Kluwer Acad., Dordrecht, Netherlands.

Peria, W. J., C. W. Carlson, R. E. Ergun, J. P. McFadden, J. Bonnell, R. C. Elphic, and R. J. Strangeway (2000), Characteristics of field-aligned currents near the auroral acceleration region: FAST observations, in *Magnetospheric Current Systems*, *Geophys. Monogr. Ser.*, vol. 118, edited by S.-I. Ohtani et al., pp. 181–189, AGU, Washington, D. C., doi:10.1029/GM118p0181.

Pottelette, R., R. A. Treumann, M. Berthomier, and J. Jasperse (2003), Electrostatic shock properties inferred from AKR fine structure, *Nonlinear Processes Geophys.*, *10*, 87–92.

Reiff, P. H., H. L. Collin, J. D. Craven, J. L. Burch, J. D. Winningham, E. G. Shelley, L. A. Frank, and M. A. Friedman (1988), Determination of auroral electrostatic potentials using high- and low-altitude particle distributions, *J. Geophys. Res.*, *93*(A7), 7441–7465, doi:10.1029/JA093iA07p07441.

Reiff, P. H., G. Lu, J. L. Burch, J. D. Winningham, L. A. Frank, J. D. Craven, W. K. Peterson, and R. A. Heelis (1993), On the high- and low-altitude limits of the auroral electric field region, in *Auroral Plasma Dynamics*, *Geophys. Monogr. Ser.*, vol. 80, edited by R. L. Lysak, pp. 143–154, AGU, Washington, D. C., doi:10.1029/GM080p0143.

Rème, H., et al. (2001), First multispacecraft ion measurements in and near the Earth's magnetosphere with the identical Cluster Ion Spectrometry (CIS) experiment, *Ann. Geophys.*, *19*, 1303–1354.

Runov, A., et al. (2005), Electric current and magnetic field geometry in flapping magnetotail current sheets, *Ann. Geophys.*, *23*, 1391–1403.

Sadeghi, S., G. T. Marklund, T. Karlsson, P.-A. Lindqvist, H. Nilsson, O. Marghitu, A. N. Fazakerley, and E. A. Lucek (2011), Spatio-temporal features of the auroral acceleration region as observed by Cluster, *J. Geophys. Res.*, *116*, A00K19, doi:10.1029/2011JA016505.

Sonnerup, B. U. Ö., and L. J. Cahill, Jr. (1967), Magnetopause structure and attitude from Explorer 12 observations, *J. Geophys. Res.*, *72*(1), 171–183, doi:10.1029/JZ072i001p00171.

Sonnerup, B. U. Ö., and M. Scheible (1998), Minimum and maximum variance analysis, in *Analysis Methods for Multi-Spacecraft Data, ISSI Sci. Rep. Ser. 001*, edited by G. Paschmann and P. W. Daly, pp. 185–220, Int. Space Sci. Inst., Bern.

Temerin, M., C. Cattell, R. Lysak, M. Hudson, R. B. Torbert, F. S. Mozer, R. D. Sharp, and P. M. Kintner (1981), The small-scale structure of electrostatic shocks, *J. Geophys. Res.*, *86*(A13), 11,278–11,298, doi:10.1029/JA086iA13p11278.

Thorne, R. M., B. Ni, X. Tao, R. B. Horne, and N. P. Meredith (2010), Scattering by chorus waves as the dominant cause of diffuse auroral precipitation, *Nature*, *467*, 943–946, doi:10.1038/nature09467.

Tsyganenko, N. A., and D. P. Stern (1996), Modeling the global magnetic field of the large-scale Birkeland current systems, *J. Geophys. Res.*, *101*(A12), 27,187–27,198, doi:10.1029/96JA02735.

Watt, C. E. J., R. Rankin, I. J. Rae, and D. M. Wright (2005), Self-consistent electron acceleration due to inertial Alfvén wave pulses, *J. Geophys. Res.*, *110*, A10S07, doi:10.1029/2004JA010877.

Wild, J. A., T. K. Yeoman, P. Eglitis, and H. J. Opgenoorth (2000), Multi-instrument observations of the electric and magnetic field structure of omega bands, *Ann. Geophys.*, *18*, 99–110, doi:10.1007/s00585-000-0099-6.

Wild, J. A., et al. (2011), Midnight sector observations of auroral omega bands, *J. Geophys. Res.*, *116*, A00I30, doi:10.1029/2010JA015874.

Wygant, J. R., et al. (2000), Polar spacecraft based comparisons of intense electric fields and Poynting flux near and within the plasma sheet-tail lobe boundary to UVI images: An energy source for the aurora, *J. Geophys. Res.*, *105*(A8), 18,675–18,692, doi:10.1029/1999JA900500.